Available online at www.sciencedirect.com

SciVerse ScienceDirect

Procedia Computer Science 00 (2012) 000–000

Procedia Computer Science

www.elsevier.com/locate/procedia

International Conference on Computational Science, ICCS 2013

Seismic Image Restoration Using Nonlinear Least Squares Shape Optimization

Mathieu Gilardet[a,b,*], Sebastien Guillon[a], Bruno Jobard[b], Dimitri Komatitsch[c]

[a] *TOTAL, Pau, France*
[b] *LIUPPA, University of Pau, France*
[c] *LMA, CNRS UPR 7051, Centrale Marseille, France*

Abstract

In this paper we present a new method for seismic image restoration. When observed, a seismic image is the result of an initial deposit system that has been transformed by a set of successive geological deformations (flexures, fault slip, etc) that occurred over a large period of time. The goal of seismic restoration consists in inverting the deformations to provide a resulting image that depicts the geological deposit system as it was at a previous state. Providing a tool that quickly generates restored images helps the geophysicists to recognize geological features that may be too seriously altered in the observed image.

The proposed approach is based on a minimization process that expresses geological deformations in term of geometrical constraints. A quickly converging Gauss-Newton approach is used to solve the system.

Results are provided to illustrate the seismic image restoration process on real data and we present how the restored version can be used in a geological interpretation framework.

Keywords: Seismic image restoration, least squares minimization process, Gauss-Newton solver.

1. Introduction

In this paper we present a new method for seismic images restoration in order to help geophysicists in their interpretation of the sedimentary deposit system. In oil and gas exploration, seismic images are acquired by propagating, recording and processing acoustic waves underground. These images highlight geological events such as *horizons* (stratigraphic limits) or *faults* (discontinuities). Because of the structural deformations of the underground that has occurred over time, such as flexure or displacements along faults, important geological structures might be difficult to detect and reconstruct (see figure 1). Our aim is to provide an easily configurable restoration tool that corrects the structural deformations to facilitate the identification of subtle geological events. The seismic restoration consists in finding a set of successive transformations between the observed image, and an *unwarped* version that represents the initial sedimentary deposit system.

Two types of deformation operation might successively intervene during the restoration process. One operation is to split a seismic image along a geological fault and to slide one resulting block along this fault in order to get

*Corresponding author. Tel.: +33-559-835518.
E-mail address: mathieu.gilardet@gmail.com.

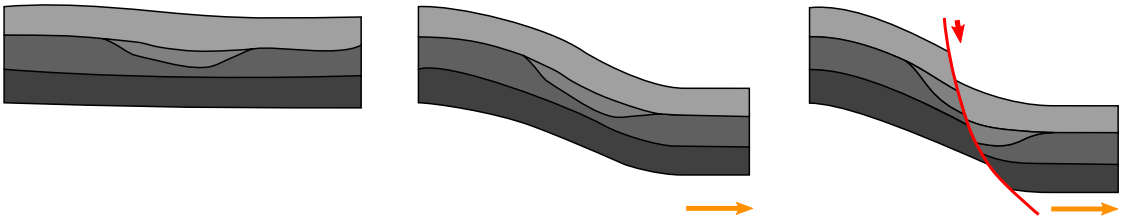

Fig. 1. **Successive geological deformations of the underground.** Over time, the structure of an initial sedimentary deposit (a) is deformed under the action of the tectonic constraints (b) that might lead to fault formation and blocks displacements (c). To facilitate understanding the resulting structure the geophysicists apply several **restoration processes** that transforms it in the opposite order ($c \rightarrow b$: *displacement along the fault*, then $b \rightarrow a$: *horizon flattening*) to recover the initial deposit system.

the horizons matching on each side of the fault (see figure 1, $c \rightarrow b$). The second operation is to deform the whole seismic image so that a selected horizon gets flattened along with the surrounding blocks, therefore restoring the initial structure of the geological deposit (see figure 1, $b \rightarrow a$).

In the domain of seismic imagery, different solutions [1], [2], [3] and [4] have been proposed to globally restore a seismic image. All these solutions are based on automatic image analysis, estimating the local dip of each horizon and then providing a global flattening process. This approach is effective as long as the seismic quality is good enough over the whole domain and that no structural deformation such as faults has altered the underground configuration. This last aspect is a major limitation since interesting geological regions are very likely to present such faults.

The geomechanical aspects of fault restoration is of a great interest for modelling and understanding a deformation process [5], [6]. The objective here concerns the quantification of the deformation history and the strain analysis. Based on geometric assumptions and mechanical rocks properties, the restoration problem is solved by a geomechanical approach. The methodology requires first to define a mesh conforming to geological interface (fault and horizons), associate mechanical properties to rock units and finally based on boundary conditions, use a finite element approach to solve the problem. These approaches does not completely suit our restoration needs, as they require to provide geomechanical properties that are not available at the early stage of the structural interpretation of seismic images. We therefore cast our attention to lighter geometrical methods that provide acceptable geological deformations without the need of injecting explicit geomechanical properties to initiate the process.

In the computer graphics field, more general purpose shape deformation techniques are able to achieve physically plausible deformation results [7], [8]. Weng et al. proposed a 2D shape deformation method that preserves the boundary curve of the shape and the local areas inside the shape [9]. The preservation of the geometrical constraints is expressed as a nonlinear least squares minimization and is resolved iteratively with a Gauss-Newton method.

Our restoration technique is an adaptation of Weng et al.'s approach. Their purely geometrical local areas preservation scheme as proven to be sufficient to mimics the geological deformation behavior in the context of seismic image interpretation. We extended their shape deformation algorithm by defining two supplementary *restoration constraints* that control the fault restoration and the horizon flattening operations.

The paper is organized as follows. Section 2 presents the general shape deformation framework. Then we introduce in the section 3 the specific constraints responsible for the fault restoration and the horizon flattening. The section 4 finally presents applications and results.

2. Shape Deformation Framework

In this section we present the global scheme of shape deformation as proposed in [9]. This scheme is based on a mesh deformation: initial mesh is obtained by a triangulation of input domain and is transformed in order to minimize a set of criteria.

Two families of criteria will be introduced to define which points should be transformed (restoration constraints) and how the transformation is extended to other points (geometrical constraints). This combination will produce a non linear system solved by a Gauss-Newton approach.

Finally using texture mapping will directly provide the transformed image on the deformed mesh.

In the following, we note $\mathcal{V}$ the set of nodes belonging to the mesh $\mathcal{M}$ and $\mathcal{V}_p$ the subset of $\mathcal{V}$ containing the nodes from the contour of $\mathcal{M}$. $\mathcal{V}_g$ is the subset of interior nodes, that does not belong to $\mathcal{V}_p$. $\mathcal{V}$ has n elements.

2.1. Restoration Constraints

The basic mechanism of shape deformation consists in defining one or several constraints that are applied to different subsets of the mesh vertices. Each constraint will be applied to a subset of vertices $\mathcal{V}_c = \{v_c\} \in \mathcal{V}$. Considering a function c that provides the new positions of a set of vertices depending on their current position, the transformation of the set of vertices can be expressed as:

$$CV = c(V) \tag{1}$$

with

- C is a $(card(\{v_c\}) \times n)$ matrix, such that $C_{r,c} = 1$ when v_c is the r^{th} element of $\mathcal{V}_c$ and the c^{th} the element of $\mathcal{V}$; $C_{r,c} = 0$ otherwise.
- V is the $(n \times 2)$ vertices matrix, such as: $\forall v_k \in \mathcal{V}, V_k = [v_{kx}, v_{ky}]$

The previous geometrical transformation can be expressed as a geometrical constraint by considering the new positions $c(V)$ as a target to reach. The deformation process will then try to minimize the difference between the current and the target positions. Therefore, we write the restoration constraint J_C to minimize as:

$$J_C = \|CV - c(V)\|^2 \tag{2}$$

In section 3, we will describe how to adapt J_C to insert the two constraints responsible for the *fault restoration* and the *horizon flattening*.

2.2. Geometrical Constraints

After having described how to impose constraints onto specific subsets of vertices, we now describe how the deformation will be propagated into the entire mesh. It is indeed important the deformation to be as uniformly distributed as possible to avoid localized distortions. This is the role of what we call the *geometrical constraints* which tend to preserve each triangle's shape and area. As stated in [9] this objective is achieved by preserving the *mean value coordinates*, the *contour Laplacian* and *edge lengths*. The following sections describe the formulation of these constraints.

2.2.1. Mean Value Coordinate

For each point v_i of $\mathcal{V}_g$ and $v_{i,j}$ its adjacent neighbors, its mean value coordinate [10], is defined as the set of $\omega_{i,j}$ weights such as:

$$v_i = \sum \omega_{i,j} * v_j \tag{3}$$

with

$$\omega_{i,j} = \frac{\lambda_{i,j}}{\sum_j \lambda_{i,j}} \ , \ \lambda_{i,j} = \frac{tan(\alpha_{j-1}/2) + tan(\alpha_j/2)}{|v_i - v_j|} \tag{4}$$

and α_j is the angle between $[v_i v_j]$ and $[v_i v_{j+1}]$.

The mean value coordinate over the entire shape can be written in matrix form as:

$$MV = 0 \tag{5}$$

with

- M a $(card(\mathcal{V}_g) \times n)$ matrix such that:
  - $M_{r,c} = \omega_{i,j}$ when v_i is the r^{th} element of $\mathcal{V}_g$, and v_j is the c^{th} element of $\mathcal{V}$.
  - $M_{r,c} = -\sum \omega_{i,j}$ when v_i is the r^{th} element of $\mathcal{V}_g$, and the c^{th} element of $\mathcal{V}$.
  - $M_{r,c} = 0$ otherwise.
- V the vertices matrix.

Preserving the mean value coordinate during shape deformation will consist in minimizing:

$$J_M = ||MV||^2 \tag{6}$$

2.2.2. Contour Laplacian

For each contour point $v_i \in \mathcal{V}_p$, mean value coordinate could induce undefined value. For this reason a Laplacian coordinate δ_i is estimated on the initial mesh:

$$\delta_i = \mathcal{L}_p(v_i) = v_i - (v_{i-1} + v_{i+1})/2 \tag{7}$$

And δ_i is introduced as a constraint to be preserved. Written for all $v_i \in \mathcal{V}_p$, we minimize:

$$J_L = \sum_{v_i \in \mathcal{V}_p} ||\mathcal{L}_p(v_i) - \delta_i||^2 = ||\Delta V - \delta(V)||^2 \tag{8}$$

with

- Δ the $(card(\mathcal{V}_p) \times n)$ matrix with
  - $\Delta_{r,c} = -1/2$ when v_i is the r^{th} element of $\mathcal{V}_p$, and v_{i-1} or v_{i+1} is the c^{th} element of $\mathcal{V}$.
  - $\Delta_{r,c} = 1$ when v_i is the r^{th} element of $\mathcal{V}_p$, and c^{th} the element of $\mathcal{V}$.
  - $\Delta_{r,c} = 0$ otherwise.
- V the vertices matrix.
- $\delta(V)$ the function that returns the $(2 \times card(V_p))$ matrix: $\delta(v_i) = T_i \delta(v_i^0)$, such that:
  - v_i^0 is the position of v_i before deformation.
  - T_i is the transformation matrix defined by: $T_i = \sum_{(i,j) \in \mathcal{E}_p} (v_j - v_i)(v_j^0 - v_i^0)^T D_i$
  - $D_i = (\sum_{(i,j) \in \mathcal{E}_p} (v_j - v_i)(v_j^0 - v_i^0)^T)^{-1}$

2.2.3. Edge Length Preservation

Mean value coordinates ensure the preservation of the triangle shape but because this measurement is invariant to the scale, a constraint on edge length must be introduced to ensure the area preservation. Preserving edge lengths requires to minimize the following energy:

$$J_E = \sum_{(i,j)\in\mathcal{E}} \|(v_i - v_j) - e(v_i, v_j)\|^2 \tag{9}$$

with

$$e(v_i, v_j) = \frac{{l_{i,j}}^0}{l_{i,j}} \tag{10}$$

where $l_{i,j}$ is the current length, and ${l_{i,j}}^0$ the length before deformation.

We rewrite (9) into the matrix form:

$$J_E = \|LV - l(V)\|^2 \tag{11}$$

with

- L the $(card(\mathcal{E}) \times n)$ oriented incidence matrix.
- V the vertices matrix.
- $l(V)$ the function that returns the $(card(\mathcal{E}) \times 2)$ matrix, where the k^{th} rows represents the k^{th} edge under its vectorial form.

2.3. Solving the System

Combining all the energy terms of restoration and geometrical constraints, the global shape deformation consists in minimizing:

$$J = \alpha J_M + \beta J_L + \gamma J_E + \zeta J_C \tag{12}$$

or:

$$J = \alpha \cdot \|MV\|^2 + \beta \cdot \|\Delta V - \delta(V)\|^2 + \gamma \cdot \|LV - l(V)\|^2 + \zeta \cdot \|CV - c(V)\|^2 \tag{13}$$

The global energy can be rewritten in a simple matrix form as:

$$min\ \|AV - b(V)\|^2, \text{ with } A = \begin{bmatrix} \alpha \cdot M \\ \beta \cdot \Delta \\ \gamma \cdot L \\ \zeta \cdot C \end{bmatrix},\ b(V) = \begin{bmatrix} 0 \\ \beta \cdot \delta(V) \\ \gamma \cdot l(V) \\ \zeta \cdot c(V) \end{bmatrix} \tag{14}$$

As minimizing J is not a linear system, a Gauss-Newton approach is used to solve it iteratively. Thus at each iteration, the following system is solved:

$$\min_{t+1} \|AV^{t+1} - b(V^t)\|^2 \tag{15}$$

Where V_t is the current positions, and V_{t+1} the updated positions on next iteration. Equation 15 is then linearized using the formulation:

$$V^{t+1} = (A^T A)^{-1} A^T b(V^t) \tag{16}$$

As A only depends on the mesh before deformation, the term $(A^T A)^{-1} A^T$ is computed once at the beginning. Therefore a single matrix multiplication is needed at each iteration. In practice, convergence appears after a hundred iterations.

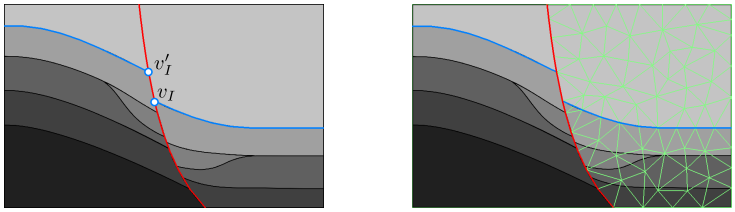

(a) (b)

Fig. 2. **Restoration workflow applied to a seismic image.** (a) Initial model (b) Meshed model.

3. Fault Restoration and Horizon Flattening Workflow

We introduce now the specific constraints responsible for the fault restoration and the horizon flattening. They are the two restoration constraints introduced in the section 2.1. To better explain the workflow, we will apply it to the synthetic test case illustrated in figure 2.a. In this case, we have identified a fault (in red) and a horizon (in blue) and the objective is to first recover from the displacement along the fault and then, in a second restoration stage, flatten the horizon.

3.1. Fault Restoration Procedure

To restore a fault displacement, a mobile block is defined on one side of the fault while the other block on the other side of the fault remains static. We then need to define two constraints controlling the displacement of the mobile block. The first constraint keeps the mobile block in contact with the fault while the second one is responsible for its displacement until the blue horizon coincides in both side of the fault.

3.1.1. Meshing of the mobile block

We start meshing the mobile block from its contour (see figure 2.b.). Before meshing make sure to insert the intersection point v_I of the blue horizon in the mobile block with the fault. We will need it later to stitch the mobile block's horizon with the corresponding point v'_I in the static bloc.

3.1.2. Fault Sliding Constraint

This first constraint must guarantee that the moving block will remain in contact with the fault during its deformation. Let $\mathcal{V}_F = \{v_F\}$ be the subset of $\mathcal{V}$, containing the vertices of the moving block laying on the fault. We define $f(v_F)$ their projection target on the fault polyline. The cumulated distance to the fault we need to minimize is:

$$J_{F1} = \sum_{v_F \in \mathcal{V}_F} (v_F - f(v_F))^2 = \|C_F V - c_F(V)\|^2 \tag{17}$$

where

- C_F is a $(card(\mathcal{V}_F) \times n)$ matrix such that $C_{F_{r,c}} = 1$ when v_F is the r^{th} element of $\mathcal{V}_F$ and the c^{th} the element of $\mathcal{V}$; $C_{F_{r,c}} = 0$ otherwise.
- V is the vertices matrix
- $c_F(V)$ is the function that returns the $(card(\mathcal{V}_F) \times 2)$ matrix that contains at the k^{th} row $[f(v_F)_x, f(v_F)_y]$.

We mention that we exclude from $\mathcal{V}_F$ the vertex v_I, which will receive a particular treatment in the next section.

3.1.3. Horizon Stitching Constraint

This constraint aims at moving the mobile block so that its v_I point gets as close as possible to the v'_I point on the border of the static block. The energy term is:

$$J_{F2} = (v_I - v'_I)^2 = \|C_I V - c_I\|^2 \tag{18}$$

with

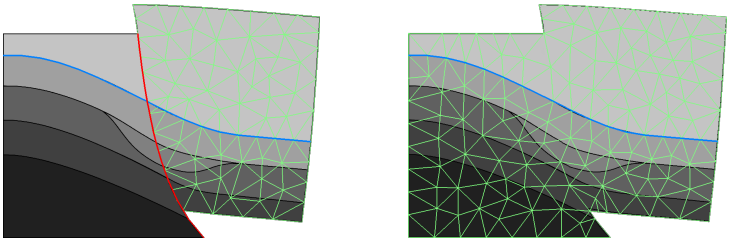

(a) (b)

Fig. 3. **Fault restored model.** (a) After the fault restoration (b) The remeshed domain for the horizon flattening process.

- C_I the $(1 \times n)$ matrix such that $C_{I0,c} = 1$ when v_I is the c^{th} element of $\mathcal{V}$; 0 otherwise.
- V, the vertices matrix.
- c_I the (1×2) target position $c_I = [v'_{Ix}, v'_{Iy}]$.

3.1.4. Gathering the Fault Restoration Constraints

From the equation 12 the global energy that has to be minimized to restore the fault is expressed by:

$$J1 = \alpha J_M + \beta J_L + \gamma J_E + \zeta J_{F1} + \lambda J_{F2} \tag{19}$$

The figure 3.a shows the result expected at the end of the fault restoration process. The mobile block is still in contact with the fault and the blue horizon is now continuous across the fault.

3.2. Horizon Flattening Procedure

This part presents the second deformation process in our restoration workflow: the flattening of a horizon. Its aim is to provide an unfolded representation of the sedimentary deposit system. For this purpose, a horizon is selected and adequate constraints will tend to flatten it. An additional constraint will take care of preserving the horizon length during the operation.

3.2.1. Whole Domain Remeshing

At this stage, the fault displacement has been restored and the selected horizon is continuous across the whole domain. We need a new mesh to start this new deformation stage. The whole domain is therefore remeshed from its contour and the selected horizon. However the previously selected fault is now ignored.

3.2.2. Horizon Flattening Constraint

Let $\mathcal{V}_H = \{v_{Hk}\ (x_k, y_k)\}$ to be the set of vertices belonging to the selected horizon. This constraint consists in displacing the v_{Hk} vertices on the selected horizon toward an horizontal line of equation $y = y_H$. Flattening the horizon will require minimizing this energy:

$$J_{H1} = \sum_{v_k \in \mathcal{V}_H} (y_k - y_H)^2 = \|C_H V = c_H(V)\|^2 \tag{20}$$

where

- C_H is a $(card(\mathcal{V}_H) \times n)$ matrix such that $C_{Hr,c} = 1$ when v_k is the r^{th} element of $\mathcal{V}_F$ and the c^{th} the element of $\mathcal{V}$; $C_{Fr,c} = 0$ otherwise.
- V is the vertices matrix
- $c_H(V)$ is the function that returns the $(\mathcal{V}_F \times 2)$ matrix that contains at k^{th} row: $[v_{kx}, y_H]$.

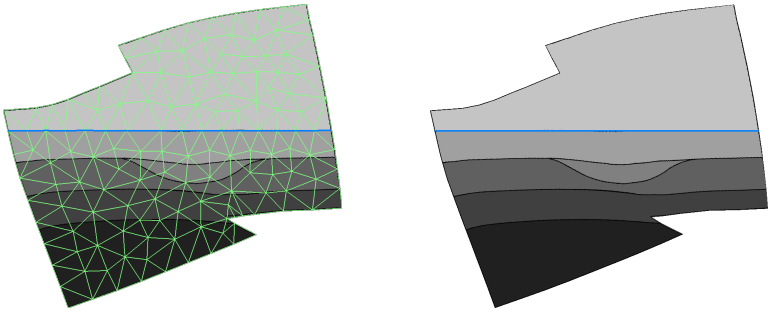

(a) (b)

Fig. 4. **Restored model after flattening.** (a) Meshed (b) Plain.

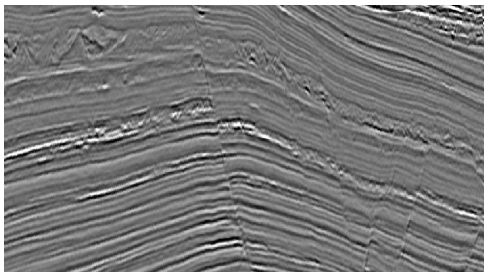

Fig. 5. **An initial seismic image** that has to be restored.

3.2.3. Horizon Length Constraint

Expressing the horizon edge's length variation consists in expressing the sum of length changes of its edges $\mathcal{E}_H$. Similarly to the equation 11, we write:

$$J_{H2} = \|L_H V = l_H(V)\|^2 \tag{21}$$

where this time, L_H and $l_H(V)$ have $card(\mathcal{E}_H)$ rows.

However, since we want to explicitly formulate the horizon length energy, the regular length expression $\|LV - l(V)\|^2$ must now exclude the set of horizon edges $\mathcal{E}_h$.

3.2.4. Gathering the Horizon Flattening Constraints

From the equation 12 the global energy that has to be minimized to flatten the horizon is expressed by:

$$J2 = \alpha J_M + \alpha J_L + \gamma J_E + \zeta J_{H1} + \lambda J_{H2} \tag{22}$$

The figure 4 shows the flattened version of the figure 3.b.

The complete restoration process shows how the special geological feature that was split by the fault on the figure 2.a has been recovered. Its visual identification is now easier.

4. Results

In this section we present the effects of the restoration processes on the real seismic image depicted in the figure 5. On this image, the objective will consist in restoring the main fault (discontinuity in the middle of the image) and unfolding the dome structure. The restoration will enable to have a better understanding of the initial deposit system and to clarify horizon continuity through the actual fault.

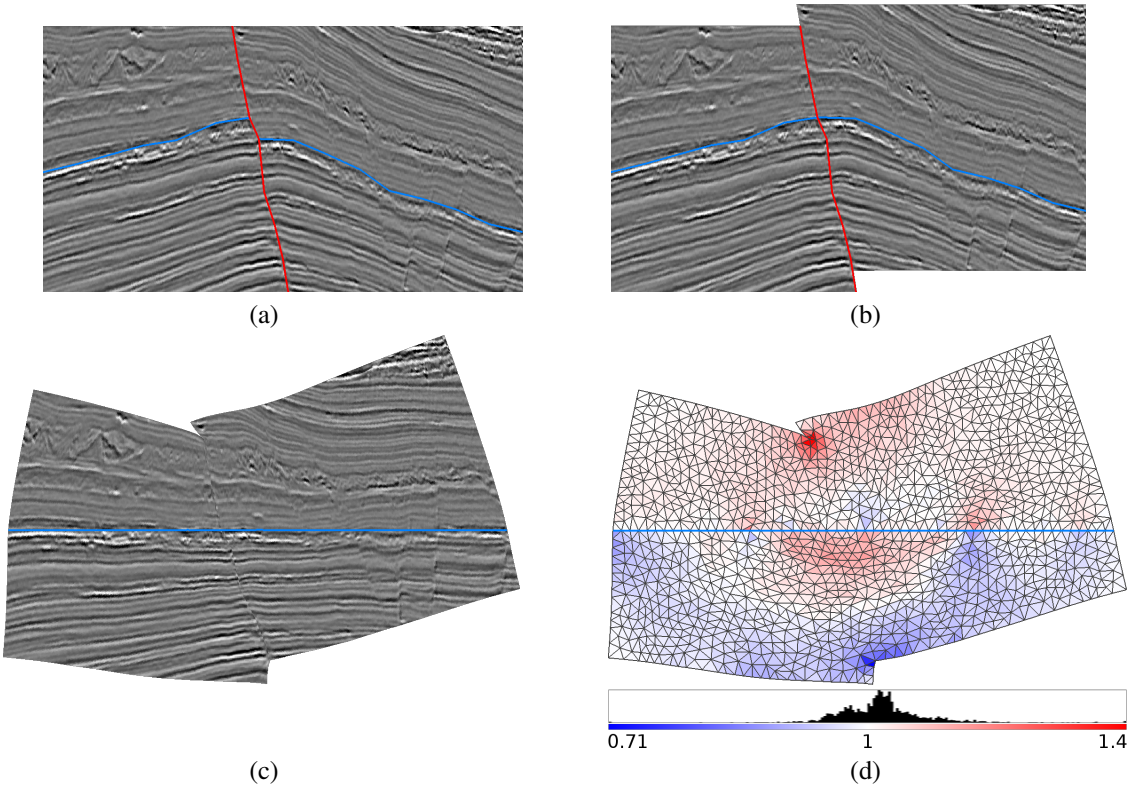

Fig. 6. **Restoration workflow applied to a seismic image.** (a) Interpreted image (b) Fault restoration (c) Final image (d) Deformation map and histogram: red shows compression, blue shows dilatation.

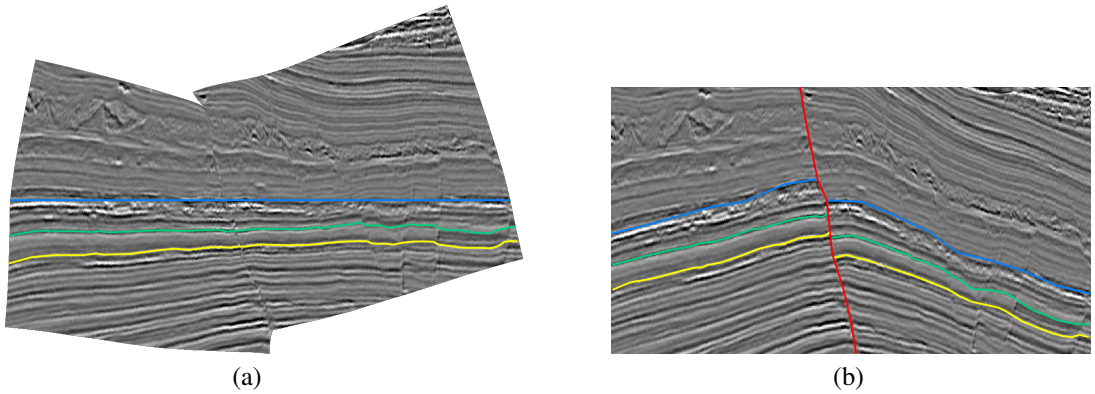

Fig. 7. **Interpreting simultaneously on both restored and original domains.** The original and restored images are connected through a bijective transformation. Therefore picking horizons on the restored domain (a) can interactively be displayed on the original domain (b).

The figure 6 shows the successive deformations of the seismic image passing through the global restoration framework. First an horizon and a fault are selected on the seismic (blue and red lines in figure 6.a). The block on the right of the fault is then restored as explained in section 3.1 and the result is displayed in figure 6.b. Finally the blue horizon is flattened as explained in section 3.2 and the resulting image is presented in figure 6.c. At this stage, the interpreters can more easily track continuous and flat horizons and eventually recognize geological features.

As a consequence of the competing constraints, the least squared minimization method usually cannot fully respect all of them. The figure 6.d shows the deformation ratio of each triangle (initial area over final area). The map thus depicts the typical regions of compression (red) and dilatation (blue) that inevitably occur during such restoration operations. The histogram distribution of the deformations attests that the minimization behaves well since most of the triangles undergo only small distortions.

It appears through our experiments that fixing weighting coefficients in a ratio of 10 between restoration constraints and geometrical constraints produces good restoration result. It means that we choose for equations 19 and 22: $\alpha, \beta, \gamma = 1$ and $\zeta, \lambda = 10$. Moreover we have observed a good stability of the restoration when applying local variations on these coefficients.

Dealing with the deformation of triangular meshes implies that the restoration process is intrinsically bijective and therefore the inverse transformation is available. It leads to an interesting tools for interpreters: they can focus their picking in the restored domain and their work will be automatically transformed in the original domain. We illustrate this possibility in figure 7 where the yellow and green horizons picked on restored domain (figure 7.a) have been transformed in the original domain (figure 7.b).

Conclusion

In this paper we have presented a complete shape deformation framework that achieves seismic image restoration based on a non linear least squares optimization. Due to the deformations expressed as purely geometrical constraints, our method is much simpler to parameterize than geomechanical based restoration approaches which require providing rocks properties. Though, we obtain results that are good enough to perform seismic interpretation tasks directly on the restored images.

Our method is fast enough for using it in interactive interpretation sessions and many restoration hypothesis can be experimented rapidly. This is particularly useful when restoring a fault, to try several feature matching positions.

In a future work, we plan to extend this framework to 3D image restoration since the underlying equations are not restricted to the 2D domain.

References

[1] N. Keskes, S. Guillon, M. Donias, P. Baylou, F. Pauget, Method of chronostratigraphic interpretation of a seismic cross section or block (2004).
[2] J. Lomask, A. Guitton, S. Fomel, J. Claerbout, A. Valenciano, Flattening without picking, Geophysics 71 (4) (2006) 13–20.
[3] V. Toujas, M. Donias, D. Jeantet, S. Guillon, Y. Berthoumieu, A robust framework for geotime cube, in: ICIP'08, 2008, pp. 1880–1883.
[4] G. Zinck, M. Donias, S. Guillon, O. Lavialle, Discontinuous seismic horizon tracking based on a poisson equation with incremental dirichlet boundary conditions., in: B. Macq, P. Schelkens (Eds.), ICIP, IEEE, 2011, pp. 3385–3388.
[5] I. Moretti, F. Lepage, M. Guiton, Kine3d: a new 3d restoration method based on a mixed approach linking geometry (2006).
[6] P. Durand-Riard, G. Caumon, P. Muron, Balanced restoration of geological volumes with relaxed meshing constraints, Comput. Geosci. 36 (4) (2010) 441–452.
[7] S. Gibson, B. Mirtich, A survey of deformable modeling in computer graphics, Technical Report TR-97-1 9.
[8] T. Igarashi, T. Moscovich, J. Hughes, As-rigid-as-possible shape manipulation, in: ACM Transactions on Graphics (TOG), Vol. 24, ACM, 2005, pp. 1134–1141.
[9] Y. Weng, W. Xu, Y. Wu, K. Zhou, B. Guo, 2d shape deformation using nonlinear least squares optimization, Vis. Comput. 22 (9) (2006) 653–660.
[10] M. S. Floater, Mean value coordinates, Comput. Aided Geom. Des. 20 (1) (2003) 19–27.